The Numerical Prediction of the Micro Climate Change by a Residential Development Region

Eun-Joo Oh, Hwa Woon Lee, Akira Kondo*, Akikazu Kaga*
and Katsuhito Yamaguchi**

Dept. of Atmospheric Sciences., Pusan National University, Busan 609-735, Korea
*Dept. of Environmental Engineering, Osaka University, Osaka 656-0871, Japan
**Dept. of Global Architecture, Osaka University, Osaka 656-0871, Japan

We developed a numerical model that considered the influences on the thermal environment of vegetation, water surfaces and buildings to predict micro climatic changes in a few km^2 scales; and applied this model to the Mino residential development region in Osaka Prefecture by using a nested technique. The calculated temperatures and winds in the residential development region reasonably agreed with the observed ones. We then investigated the influences on the thermal environment of the construction of a dam, the change of the green coverage rate. The results obtained from the numerical simulations were qualitatively reasonable.

Key words : Micro climate, Nested technique, Urban canopy, Numerical model

1. Introduction

In a residential development the ground surface changes from one of vegetation to one of artificial structures, the amount of the artificial heat caused by human activities increases, and the residential development has the potential to cause a micro climate change. In recent years it has been required of developments that not only the micro climate influences are suppressed, but a good environment is also created by positively using natural resources such as water, vegetation or geographical features. In Village Homes, USA or Stuttgart, Germany[1], such trials have already been carried out. In especially Germany, "climaatlas" which is a map for wind and climate is prepared for urban planning and the inclusion about environmental issues is required for urban planning. This concept has been introduced in Japan through "Japanese - German

Corresponding Author : Hwa Woon Lee, Dept. of Atmospheric Sciences, Pusan National University, Busan 609-735, Korea
Phone : +82-51-510-2291
E-mail : hwlee@pusan.ac.kr

Symposium"[2], in which several examples about use of "climaatlas" were described. The trials based on such concept are beginning to be tried in some residential developments in Japan.[3] proposed the new concept "climatopes" for optimizing urban planning processes and applied it to Basel. If the influences of the development on the thermal environment can be predicted in advance, we can compare alternative plans and development changes making it possible for these influences to be reflected in the residential development. The influence on the thermal environment of the elements of water and vegetation[4], and buildings[5] have already been researched in measurement studies and model simulations.[6,7] elucidated the heat island phenomenon by use of a meso-scale numerical model.[8] applied the numerical model developed for the vegetation canopy layer (Wilson, 1977) to the urban canopy layer, and elucidated the atmospheric and thermal environment in the urban canopy. However there are few examples of studies that have compounded the influences of each element of a residential development.

In this paper, we developed a numerical

simulation model that could predict diurnal flow and temperature variations in a few km^2 scales; and applied this model to the Mino residential development area to confirm the validity of the model. Moreover, we investigated the effect of the microclimate changes of this residential development.

2. Numerical model

A nesting technique was used to take into account the synoptic influence of the development area. A scale-down of four stages (large, middle, small and development scale) was performed (Fig.1). A hydrostatic model was used in the large region, while a non-hydrostatic model was used in - the other regions. The turbulence closure model Level 2.5 proposed by Mellor and Yamada[9] was used. The ground surface temperatures were determined by using both the urban canopy model, considering the heights of the buildings, and the multi-layer vegetation model in just the development region, while ground surface temperatures in other regions were determined by resolving the single-layer vegetation model proposed by Deardorff[10].

2.1. Basic equation

The hydrostatic model used here was described in A. Kondo et al.[11], and in this section the basic equation of the non-hydrostatic model used for the development region is described. The effect of the open space reduction by buildings is taken into consideration with this basic equation.

This idea had already introduced in one-dimensional urban canopy model by H. Kondo and F. H. Liu[12] and two-dimensional urban canopy model by A. Kondo et al.[13]. The introduction of this idea would induce as follows; (1) In the boundary between a grid including buildings and a grid including no buildings, the wind speed above the urban canopy becomes fast in order to satisfy mass balance. (2) When the magnitude of the heat flux generating within a grid is same, the temperature becomes high because the volume of a grid is small.

Momentum equation

$$\frac{du}{dt} = r_v f v - r_x c_p \theta \left(\frac{\partial \Pi'}{\partial x} + G_2 \frac{\partial \Pi'}{\partial z^*} \right) + D(u)$$

$$- r_v (C_{DB} \xi_u A(z) + C_{DF} \eta a(z)) u \sqrt{u^2 + v^2} \qquad (1)$$

$$\frac{dv}{dt} = -r_v f u - r_y c_p \theta \left(\frac{\partial \Pi'}{\partial y} + G_3 \frac{\partial \Pi'}{\partial z^*} \right) + D(v)$$

$$- r_v (C_{DB} \xi_v A(z) + C_{DF} \eta a(z)) v \sqrt{u^2 + v^2} \qquad (2)$$

$$\frac{dw}{dt} = g \left(\frac{\theta'}{\Theta} + 0.608 q'_v \right) - r_z c_p \theta G_1 \frac{\partial \Pi'}{\partial z^*} + D(w) \qquad (3)$$

Equation of continuity

$$\frac{\partial r_x u}{\partial x} + \frac{\partial r_y v}{\partial y} + \frac{\partial r_z w^*}{\partial z^*} + G_2 \left(\frac{\partial r_x u}{\partial z^*} - \frac{\partial r_z u}{\partial z^*} \right)$$

$$+ G_3 \left(\frac{\partial r_y v}{\partial z^*} - \frac{\partial r_z v}{\partial z^*} \right) - \frac{1}{z^* - s} (G_2 r_z u + G_3 r_z v) = 0 \qquad (4)$$
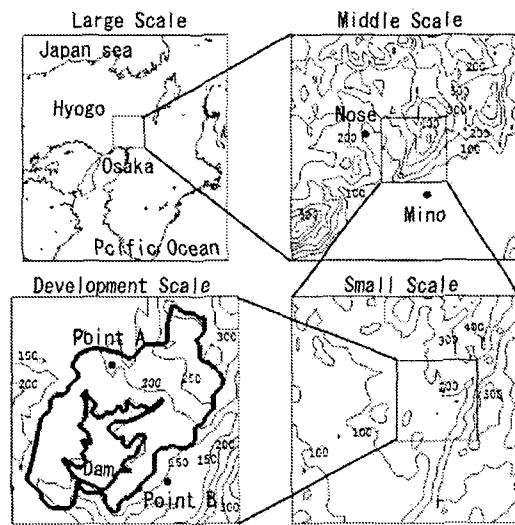

Fig. 1. Four calculated regions. The square line represents the next calculation region. The thin lines in 'middle, small and development scale' represent isoclines. The thick line in 'development scale' represents the development area. Two black circles (Nose and Mino) in 'middle scale' represent the observatories. Two black circles (Point A and B) in 'development scale' represent the observatories.

Potential temperature equation

$$\frac{d\theta}{dt} = D(\theta) + r_v \frac{1}{\rho_a c_p}(H_B + H_F + H_A) \tag{5}$$

Specific humidity equation

$$\frac{dq_v}{dt} = D(q_v) + r_v \frac{1}{\rho_a L_w}(L_w E_B + L_w E_F + L_w E_A) \tag{6}$$

Turbulence energy equation

$$\frac{d}{dt}\left(\frac{q^2}{2}\right) = D\left(\frac{q^2}{2}\right) + r_v G_1 (-\overline{u''w''})\frac{\partial u}{\partial z^*}$$

$$-\overline{v''w''}\frac{\partial v}{\partial z^*}) + r_v \beta g \overline{w''\theta''} - r_v \frac{q^3}{B_1 l}$$

$$+ r_v C_{DB} A(z)(\xi_u |u|^3 + \xi_v |v|^3)$$

$$+ r_v C_{DF} \eta a(z)(|u|^3 + |v|^3) \tag{7}$$

Turbulence length scale equation

$$l = \frac{kz}{1 + \dfrac{kz}{l_0}}, \qquad l_0 = 0.1\frac{\displaystyle\int_0^\infty zq\,dz}{\displaystyle\int_0^\infty q\,dz} \tag{8}$$

where u, v, w are the wind components of x, y, z directions, w^* the vertical wind component in the z^* coordinate, s the top height of the calculated region, f the Coriolis parameter, c_p the specific heat at a constant pressure, L_w the latent heat, ρ_a the air density, κ the Karman constant, θ the potential temperature, (Exner function, g the gravity acceleration, $\bar{\theta}$ the reference potential temperature, q_v the specific humidity, q^2 the turbulence energy, l the turbulence length scale, β the thermal expansion coefficient, B_l =15.0[-] a empirical constant, and $\cdot'$, θ', $q_v{}'$ deviations from the initial pressure, potential temperature and specific humidity respectively. $\overline{u''w''}$, $\overline{v''w''}$ are the Reynold stress, $\overline{w''\theta''}$ the heat flux, C_{DB}=0.2[-] and C_{DF} =0.2[-] a drag coefficient for buildings and vegetation, ξ_u, ξ_v a fraction of the total vertical surface area of the building perpendicular to the wind component u, v, and $A(z)$ the building surface area density function. η is a fraction of an area covered with trees, $a(z)$ a leaf surface area

density. r_v is a fraction excepting the volume occupied by buildings in a calculation mesh, and r_x, r_y, r_z fractions excepting the sections occupied by buildings in the yz, xz, xy sections in a calculation mesh, respectively. H_B , $L_w E_B$ are the sensible heat fluxes from the building surfaces, vegetation and human activities respectively and H_A , $L_w E_A$ the latent heat fluxes from the building surfaces, vegetation and human activities respectively. The terms of the sensible heat flux and the latent heat flux from human activities are neglected in these calculations.

The fifth terms on the right side in the equations (1), (2) represent the reductions of wind speeds by buildings, and the sixth term on the right side in the equation (7) represents the generation of turbulence energy by buildings

The substantial differential is defined by

$$\frac{d}{dt} = r_v \frac{\partial}{\partial t} + r_x u \frac{\partial}{\partial x} + r_y v \frac{\partial}{\partial y} + r_z w^* \frac{\partial}{\partial z^*} \tag{9}$$

The diffusion term $D(\ )$ is given by

$$D() = \frac{\partial}{\partial x}(r_x K_H \frac{\partial}{\partial x} + r_x K_H G_2 \frac{\partial}{\partial z^*})\cdot$$

$$+ G_2 \frac{\partial}{\partial z^*}(r_x K_H \frac{\partial}{\partial x} + r_x K_H G_2 \frac{\partial}{\partial z^*})$$

$$+ \frac{\partial}{\partial y}(r_y K_H \frac{\partial}{\partial y} + r_y K_H G_3 \frac{\partial}{\partial z^*})$$

$$+ G_3 \frac{\partial}{\partial z^*}(r_y K_H \frac{\partial}{\partial y} + r_y K_H G_3 \frac{\partial}{\partial z^*})$$

$$+ G_1^2 \frac{\partial}{\partial z^*}(r_z K_V \frac{\partial}{\partial z^*}) \tag{10}$$

where K_H, K_V are the horizontal and the vertical diffusion coefficients, and G_1, G_2, G_3 the differential operators to transform z coordinates into z^* coordinates given by

$$G_1 = \frac{\partial z^*}{\partial z} = \frac{s}{s - z_G}, \qquad G_2 = \frac{\partial z^*}{\partial x} = \frac{z^* - s}{s - z_G}\frac{\partial z_G}{\partial x},$$

$$G_3 = \frac{\partial z^*}{\partial y} = \frac{z^* - s}{s - z_G}\frac{\partial z_G}{\partial y} \tag{11}$$

where z_G is the ground height above sea level.

Pressure is obtained by iteration calculation of

Poisson equation that is reformed from the momentum equations. Theoretically, the divergence before one step would be zero. However, since the term becomes non-zero due to round-off errors, Poisson equation including the term is solved.

2.2. Urban canopy model

The sensible heat flux (H_B)and the latent heat flux (L_wE_B) from the building surface in the equation (5) and (6) can be obtained by resolving the energy budget equation at each height given by

$$R_{net} = G_B + H_B + L_W E_B \qquad (12)$$

where R_{net} is the net radiation flux at each height that can be obtained from the urban canopy model[14], and G_B is the heat flux onto the building surface (or the roof or ground surfaces).

The sensible heat flux and the latent heat flux are given by

$$H_B = \rho_a c_p C_H (T_i - T_a) \qquad (13)$$

$$L_W E_B = L_W \rho_a C_B u (q_{vsuf,i} - q_{v,a}) \qquad (14)$$

where C_H =0.05[-] and C_E =0.05[-] are the bulk transfer coefficients of the sensible heat flux and the latent heat flux, $q_{v,suf}$ the specific humidity on the surface , and $q_{v,a}$ and T_a the specific humidity and the temperature of the air respectively.

2.3. Multi-layer vegetation model

The sensible heat flux (H_F) and the latent heat flux (L_wE_F) from the vegetation in the equation (5), (6) can be obtained by resolving the multi-layer vegetation model. We assumed that the sensible heat flux, the latent heat flux and the net radiation flux balance at each height(the thermal storage of vegetation is neglected.), and the sensible heat flux and the latent heat fluxes are given by the Bowen ratio (B =1.0[-]).

$$a(z) = A_t \hat{a}(z'), \qquad z' = \frac{z}{h_{fc}} \qquad (15)$$

where A_t =0.8[m^2 / m^3] is the total leaf surface area density, h_{fc} the height of the vegetation and $\hat{a}(z')$ the leaf surface area density function[15]

expressed by

$$\hat{a}(z') = a_m(1 - z') \exp[\frac{1}{2}\lambda^2 - \frac{1}{2}(z' - \lambda)^2] \qquad (16)$$

where a_m is a constant determined so as to satisfy the equation(17),

$$\int_0^1 \hat{a}(z')dz' = 1 \qquad (17)$$

and λ a parameter to prescribe the vertical profile of the leaf surface area density.

The net radiation flux at each height[9] is given by

$$R_N(z) = \eta_{fc} R_{Nh}\left[\exp\{-kL(z)\} - \eta_{fc}\left(1 - \frac{z}{h_{fc}}\right)\exp\{-kL(0)\}\right] \qquad (18)$$

where η_{fc} is a fraction of the area covered with vegetation, R_{Nh} the net radiation flux above the vegetation, κ=0.2[-] the extinction coefficient and $L(z)$ the leaf area index defined by

$$L(z) = \int_z^{h_{fc}} a(z')dz' \qquad (19)$$

The sensible heat and latent heat fluxes from the vegetation are given by

$$H_F = \frac{B}{B+1}\frac{\partial R_N(z)}{\partial z} \qquad (20)$$

$$L_W E_F = \frac{1}{B+1}\frac{\partial R_N(z)}{\partial z} \qquad (21)$$

2.4. Boundary and initial conditions

The initial value of the wind velocity was given 0 in four calculated regions. The initial value of the potential temperature was given 298K at the sea level height, and the constant potential temperature gradient 0.005K/m in four calculated regions. The initial value of the specific humidity was given the relative humidity of 50% until the height of 2000m and the relative humidity of 20% over the height of 2000m. The initial values of the turbulent variables were determined from the turbulent closure Level 2 model.

The surface temperature and the specific humidity were determined by solving the ground surface heat budget equation proposed by Dear-

dorff in the large, middle and small regions, and were determined from both the urban canopy model described in the section 2.2 and the multi layer vegetation model described in the section 2.3. The bottom boundary values of the potential temperature, the specific humidity and the wind velocity were determined from the similarity theory of Monin-Obukhov. The conditions of the gradient = 0 for all variables were set to the lateral boundary in the large region. The lateral boundary values of the wind components, the potential temperature and the specific humidity in other regions were determined from the one-way nesting technique that can exactly express the complex terrain.

The calculation was performed for 48 hours from 8 a.m. on a typical summer day. The calculated results of last 24 hours were adopted. The calculation of four regions was carried out one by one and the calculated values in every hour were saved. The lateral boundary values were given by the interpolation of these data. Moreover, in order to satisfy mass conversation in the entire domain, the adjustment to the time tendency of wind component u and v is performed.

3. Input data

Four calculated regions (large, middle, small and development region) are shown in Fig.1. The region enclosed by the square in the large, middle and small regions corresponds to the next region. Two black circles in the middle region represent the AMeDAS (Automated Meteorological Data Acquisition System) observatories, Mino and Nose. Two black circles in the

development region also represent the meteorological observatories. The outside and the inside thick lines in the development region represent the residential development and dam areas, respectively. The position, area, number of the mesh and the mesh size in the four regions are shown in Table 1. The top height in all regions is 5000m. The number of the mesh in the development region and in other three regions is 23 and 15 respectively. The maximum height of buildings and trees in this calculation in the development region is 15m. The fine mesh of 3 m is adopted until 36m from the ground level to investigate the micro climate effect of the vertical structures like buildings and trees.

The topography after and before development is shown in Fig. 2. Ups and downs of a mountain become small from Fig. 2. The land-use after development is shown in Fig. 3. The inside of thick line is the development area and the shade area represents the dam area. The land-use is classified into 27 categories. The rate of road, trees, grass, soil and water surfaces and the averaged heights of the buildings and

Table 1. Definition of calculated region

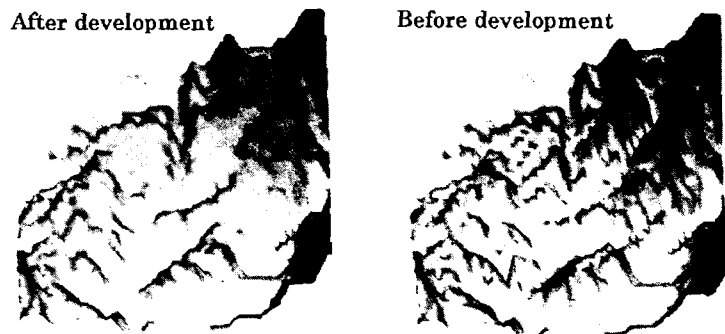| Region	Large	Middle	Small	Development
Latitude	33.50~35.94	34.72~35.03	34.84~34.92	34.87~34.90
Longitude	133.80~137.00	135.23~135.69	135.38~135.50	135.44~135.48
Area [km²]	252 × 290	39 × 39	8 × 8	3 × 3
Number of mesh	90 × 100	39 × 39	40 × 40	26 × 26
Mesh size	3 km	1 km	200 m	120 m

After development   Before development
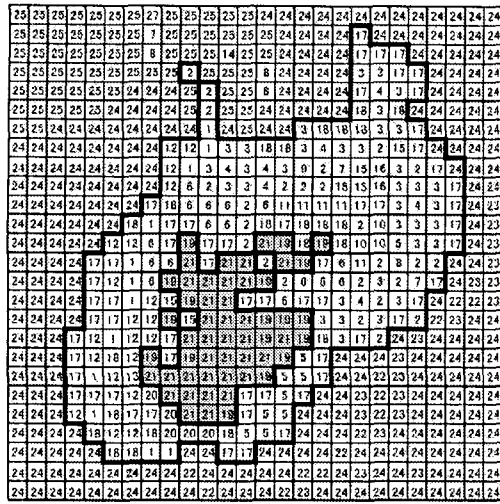

Fig. 2. Topography after and before development.

Fig. 3. Map of land-use categories after development. The thick line represents the development area. The shade represents the dam area.

trees are set up by each category. The land-use categories and rate set ups are shown in Table 2. The main land-use in 'Center area' is road and the averaged height of building is 15m. The land-use rate of 'Green' in 'Detached house 2' is the largest among house categories.

The first and second numbers in parenthesis in Table 2 express the land-use rate in the case of increasing green coverage (case 2; described later) and decreasing green coverage (case 3; described later) respectively. The land-use of the residential development area in its present state is all a forestation (the number of the land-use category is 24.).

4. Model evaluation

To verify the accuracy of this model, we extracted observed data (August 1992) for four

Table 2. Land-use categories and land-use rate

No.	Category	Road	Tree	Grass	Soil	Water	BC	BH	TH
1	Arterial road (width≥20m)	64(54,64)	18(28,6)	18	0(0,12)	0	30	6	9
2	Arterial road (width≤20m)	56(42,57)	22(36,7)	22	0(0,14)	0	40(50,40)	6	9
3	Detached house 1	76(70,100)	0(30,0)	24(0,0)	0	0	40(40,30)	6	0
4	Detached house 2	46(42,62)	10(40,10)	32(16,0)	12(2,28)	0	40(50,30)	6	9
5	Low multiple dwelling house	80(68,100)	0(32,0)	20(0,0)	0	0	60	9	0(9,0)
6	High multiple dwelling house	84(68,100)	0(32,0)	16(0,0)	0	0	60(70,50)	15	0(9,0)
7	School 1 (building)	50	10	10	30	0	80	15	9
8	School 2 (ground)	0	5	5	90	0	0	0	9
9	School 3	25	5	5	65	0	80	15	9
10	Center area 1	80(40,100)	15(60,0)	5(0,0)	0	0	90(90,70)	15	9
11	Center area	85(40,100)	10(60,0)	5(0,0)	0	0	80(90,70)	15	9
12	Center area	76(76,100)	12(12,0)	12(12,0)	0	0	50(50,40)	15	9
13	Water purification plant	80(80,100)	10(10,0)	10(10,0)	0	0	30(30,20)	15	9
14	Park 1	5	25(50,25)	40(40,0)	30(5,70)	0	0	0	9
15	Park 2	6	25(50,25)	40(40,0)	29(4,69)	0	20	3	15
16	Park 3	0	80	20(20,0)	0(0,20)	0	0	0	15
17	Green area 1	0	100	0	0	0	0	0	15
18	Green area 2	0	100	0	0	0	0	0	3
19	Dam shore	0	0	0	100	0	0	0	0
20	Dam bank	100	0	0	0	0	0	0	0
21	Dam water	0	0	0	0	100	0	0	0
22	River	10	30	50	0	10	0	0	6
23	Field	10	10	80	0	0	0	0	6
24	Green area 3*	0	100	0	0	0	0	0	15
25	Detached house 1*	76	0	24	0	0	40	6	0
26	Arterial road (width≥20m)*	64	18	18	0	0	30	6	9
27	Arterial road (width≤20m)*	56	22	22	0	0	40	6	9

* : Outside of the residence development area
BC : a fraction of an area covered with buildings, BH : height of building, TH : height of tree

conditions:

(1) The daily averaged wind speed was lower than the monthly averaged one,

(2) The amount of the averaged daily solar radiation was larger than the monthly averaged one,

(3) The daily averaged range of temperatures was larger than the monthly averaged ones,

(4) No precipitation.

Data of 8 selected days (1, 5, 16, 21, 23, 26, 28, 29) were compared with the calculated results. The diurnal wind vector variations of AMeDAS data at Mino and Nose, and the
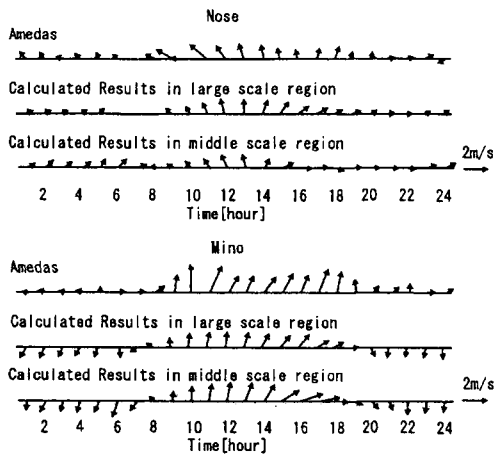

Fig. 4. Diurnal wind vector variations at 10 m height of Mino and Nose. The wind vectors of Amedas are the averaged ones of 8 days.

calculated results in the large and the middle regions are shown in Fig. 4. The wind vectors of AMeDAS are the averaged ones of selcted 8 days. It was found that the wind speed and direction in the synoptic scale generally re-appeared; though, there were a few differences about the wind direction in the night time, because the resolution of a grid is coarse to exactly express the topography. The calculated flow fields in the large and the middle regions at 14 JST are shown in Fig. 5. The sea breeze blew strongly in the coastal region on this day and penetrated deep inland. The calculated flow fields expressed this feature of the sea breeze. Next, the diurnal temperature variations of the two observatories, and the calculated results are shown in Fig. 6. The calculated wind speeds and temperatures reasonably agreed with the observed ones, making it clear that we could calculate the flow and the temperature fields in the present state using this model.

5. Sensitivity studies

To investigate the temperature change caused by the dam construction and the land-use rate, five calculations were carried out in the conditions:

case0 base plan
case1 construction of only the dam.
case2 increase of green coverage
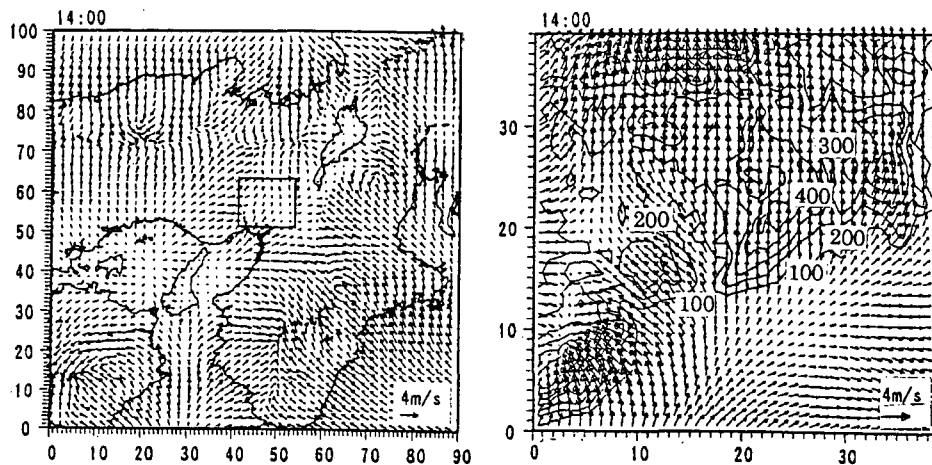case3 decrease of green coverage

Fig. 5. Flow fields at 14 JST at 12 m height in the large and the middle region. The square line represents the middle region. The thin line in the middle region represents isoclines.

5.1. Effect of dam construction

The calculation was performed adding only the construction of the dam to the present state
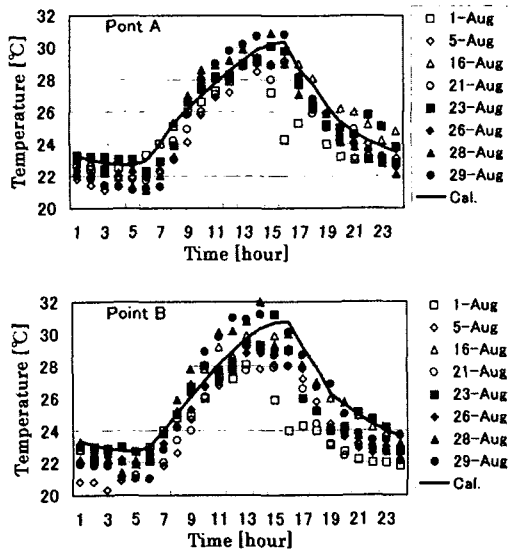

Fig. 6. Diurnal temperature variations at 10 m height of two observatories in the development region.

condition. The temperature on the dam surface was given by the equation (22) on the base of the observed temperature on the dam surface near the residential development area.

$$T_{suf} = 299 + 1.5\sin(\pi(t-9)/24) \qquad (22)$$

where t is the time. The temperature change fields between case 1 and the present state are shown in Fig. 7. The temperature around the dam decreased about 0.2℃ at 12:00, while the temperature in the leeward area was raised about 0.3℃ at 20:00. The range of temperature change is small because of little effect of the convection. However, there was almost no temperature change caused by the construction of the dam from midnight to dawn. Note that the temperature around the concrete bank was the highest.

5.2 Effect of increasing green coverage

This calculation was performed with the condition that the rate of green coverage was higher than case 0. The temperature change fields between case 2 and case 0 are shown in
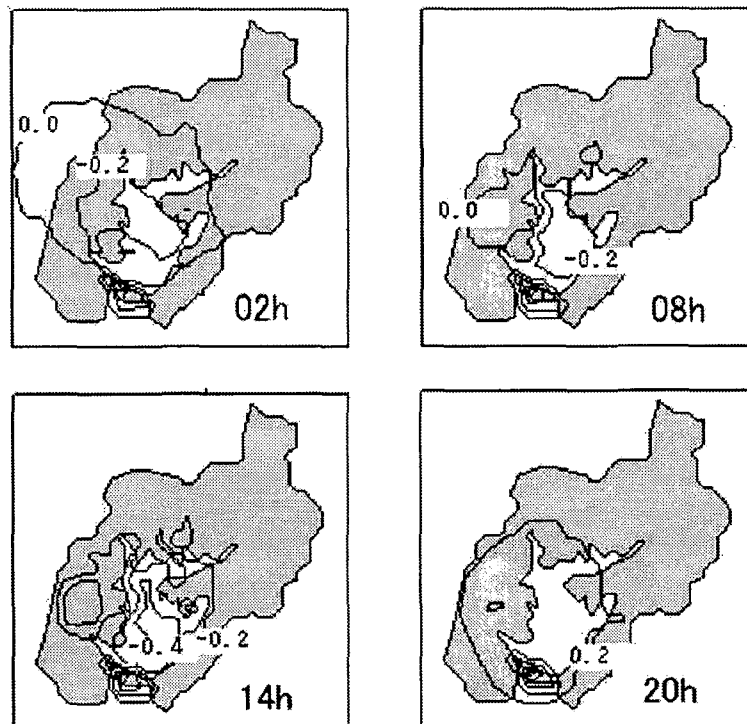

Fig. 7. Temperature change fields by dam construction. The shade represents the development area and the unit of the numerical is ℃.
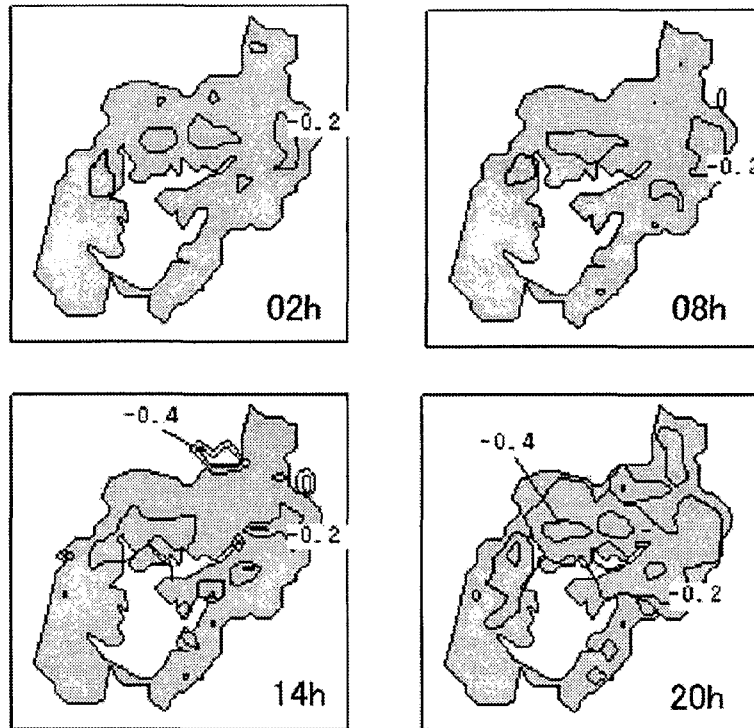
Fig. 8. Temperature change fields by increasing of the green coverage. The shade represents the development area and the unit of the numerical is °C.
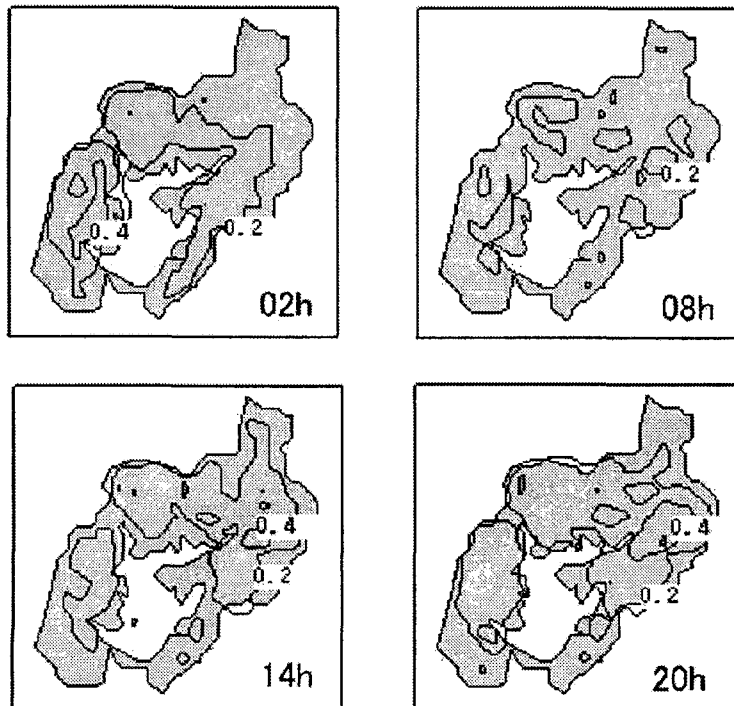

Fig. 9. Temperature change fields by decreasing of the green coverage. The shade represents the development area and the unit of the numerical is °C.

Fig. 8. The temperature in the region with increasing green coverage decreased at all times. The decrease of the temperature was especially seen in detached house (the numbers of the land-use categories were 3 and 4.) and in park (the numbers of the land-use categories were 14 and 15) from midnight to noon and was about 0.3℃. The maximum decrease of the temperature occurred between 18 JST and 22 JST in center area (the numbers of the land-use categories were 10 and 11) and was about 0.5℃. This cause was that the thermal storage at ground surface decreased due to the increase of green coverage. The vertical decrease of the temperature strongly occurred between 18 JST and 22 JST but its effect was less than 10 m from the canopy height.

5.3 Effect of decreasing green coverage

This calculation was performed with the condition that the rate of green coverage was smaller than case 0. The temperature change fields between case 3 and case 0 are shown in Fig. 9. The temperature in the region with decreasing green coverage decreased at all times. The increase of the temperature was especially seen in dwelling house (the numbers of the land-use categories were 5 and 6) and in center area(the numbers of the land-use categories were 10, 11 and 12). The maximum increase of the temperature occurred at 20 JST in center area and was about 0.6℃. The height of the vertical increase of the temperature was less than 10 m from the canopy height.

6. Conclusions

We developed a numerical model that considered the influences on the thermal environment of vegetation, water surface and buildings to predict micro climatic changes in a few km² scales; applying this model to the Mino residential development region in Osaka Prefecture. The calculated temperatures and wind speeds reasonably agreed with the observed ones, confirming the validity of this model. We also investigated the influences on the thermal environment of the construction of the dam, changes of the green coverage rate. It was found that (1) the temperature around the dam decreased about 0.2℃ from the construction of

the dam, (2) the change of the green coverage rate reduced the temperature change a maximum of 1. These results were qualitatively reasonable, but need to be examined quantitatively in the future.

Acknowledgements

References

1) Baumüller, J., U. Hoffmann and U. Reuter, 1999, Städtebauliche Klimafibel, Wirtschaftsministerium.

2) Kuttler, W., 2000, Third Japanese-German Symposium on Urban Climatology., University of Essen.

3) Scherer, D., U. Fehrenbach, H. D. Beha and E. Parlow, 1999, Improved concepts and methods in analysis and evaluation of the urban climate for optimizing urban planning processes, Atmos. Environ., 33, 4185-4193.

4) Naot, O. and Y. Mahrer, 1991, Two-Dimensional Microclimate Distribution Within and Above a Crop Canopy in an Arid Environment : Modeling and Observational Studies., Boundary-Layer Meteorol., 56, 223-244.

5) Sakakibara, Y., 1996, A Numerical Study of the Effect of Urban Geometory upon the Surface Energy Budget, Atmos. Environ., 30, 487-496.

6) Kimura, F. and S. Takahashi, 1991, The Effect of Land-use and Anthropogenic Heating on the Surface Temperature in the Tokyo Metropolitan Area: A Numerical Experiment., Atmos. Environ., 25B, 155-164.

7) Saitho, T. S., T. Shimada and H. Hoshi, 1996, Modeling and Simulation of the Tokyo Urban Heat Island, Atmos. Environ., 30, 3431-3442.

8) Uno, I., H. Ueda and S. Wakamatsu, 1989, Numerical Modeling of the Nocturnal Urban Boundary Layer, Boundary-Layer Meteorol., 49, 77-98.

9) Mellor, G. L. and T. Yamada, 1982, Development of a Turbulence Closure Model

for Geophysical Fluid Problems., Review Geophys. and Space Phys., 20, 851-875.

10) Deardorff, J. W., 1978, Efficient prediction of ground surface temperature and moisture with inclusion of a layer vegetation., J. Geophy. Res., 83, 1889-1903.

11) Kondo, A., K. Yamaguchi and H. K. Ahn, 1996, Simulation of Climatic Effects by Construction of Reclaimed Island in Pusan, Korea, Atmos. Environ., 30, 2437-2448.

2) Kondo, H. and F. H. Liu, 1998, A Study on the Urban Thermal Environment Obtained through One-Dimensional Urban Canopy Model., J. Jpn. Soc. Atmos. Environ., 33, 179-192(in Japanese).

13) Kondo, A., K. Yamaguchi and M. Ueno, 1999, Relationship between Urban Canopy Configuration and Heat Island Intensity Derived from Two-Dimensional Atmospheric Boundary Layer Model., J. Jpn. Soc. Atmos. Environ., 34, 422-434(in Japanese).

14) Kondo, A., M. Ueno, A. Kaga and K. Yamaguchi, 2001, The Influence of Urban Canopy Configuration on Net Radiation Flux., Boundary-Layer Meteorol., 100, 225-242.

15) Kondo, J. and S. Akashi, 1976, Numerical Study on the two-dimensional flow in horizontal homogeneous canopy layers, Boundary-Layer Meteorol., 10, 255-272.